Synthetic high angular momentum spin dynamics in a microwave oscillator

Saswata Roy,[1] Alen Senanian,[1] Christopher S. Wang,[2] Owen C. Wetherbee,[1] Luojia Zhang,[1] B. Cole,[3] C. P. Larson,[3] E. Yelton,[3] Kartikeya Arora,[4,5] Peter L. McMahon,[6] B. L. T. Plourde,[3] Baptiste Royer,[5,*] and Valla Fatemi[6,†]

[1] *Department of Physics, Cornell University, Ithaca, NY, 14853, USA*
[2] *James Franck Institute and Department of Physics,*
University of Chicago, Chicago, IL, 60637, USA
[3] *Department of Physics, Syracuse University, Syracuse, New York 13244-1130 USA*
[4] *Department of Physics, Indian Institute of Technology (Banaras Hindu University), Varanasi 221005, India*
[5] *Département de Physique and Institut Quantique,*
Université de Sherbrooke, Sherbrooke J1K 2R1 QC, Canada
[6] *School of Applied and Engineering Physics, Cornell University, Ithaca, NY, 14853, USA*

(Dated: March 13, 2025)

Spins and oscillators are foundational to much of physics and applied sciences. For quantum information, a spin 1/2 exemplifies the most basic unit, a qubit. High angular momentum spins (HAMSs) and harmonic oscillators provide multi-level manifolds which have the potential for hardware-efficient protected encodings of quantum information and simulation of many-body quantum systems. In this work, we demonstrate a new quantum control protocol that conceptually merges these disparate hardware platforms. Namely we show how to modify a harmonic oscillator on-demand to implement a continuous range of generators to accomplish linear and nonlinear HAMS dynamics. The spin-like dynamics are verified by demonstration of linear spin coherent (SU(2)) rotations, nonlinear spin rotations, and comparison to other manifolds like simply-truncated oscillators. Our scheme allows universal control of a spin cat logical qubit encoding with interpretable drive pulses: we use linear operations to accomplish four logical gates, and further show that nonlinear spin rotations can complete the logical gate set. Our results show how motion on a closed Hilbert space can be useful for quantum information processing and opens the door to superconducting circuit simulations of higher angular momentum quantum magnetism.

---

[*] baptiste.royer@usherbrooke.ca

[†] vf82@cornell.edu

Supplementary Information

I. ADDITIONAL EXPERIMENTS WITH SU(2) DRIVES

A. Spin locking

We can choose the (global) cavity drive phase φ to interpolate between $\hat{J}_x^{(J)}$ and $\hat{J}_y^{(J)}$ which means we can change the rotation axis on a high angular momentum spin Bloch sphere. If the spin is driven for quarter of a period of its dynamics by the $\hat{J}_x$ drive we will create an eigenstate of $\hat{J}_y$. If we turn on a $\hat{J}_y$ drive, such a spin state ideally should not change.

We show such a spin locking phenomena in Fig. S1. Since the experiment suffers from non-idealities and decoherence, we compare our spin locking with the case where the $\hat{J}_x$ drive is on for same duration. In Fig. S1(e), the measured Wigner function for the created state after applying the $\hat{J}_x$ drive for quarter period and the spin locked state look similar whereas the state created by $\hat{J}_x$ driving is different.

This spin locking phenomenon is also special to spin which is enabled by our phase tuning. Simply truncating the Hilbert space by using the frequency comb on the qubit and then changing the axis of rotation does not create such a locking phenomena. This can be seen in the cavity population and measured Wigner functions shown in Fig. S1(c, d, f). Since, our protocol suffers from the experimental non-idealities we also show the simulated population dynamics in an ideal system where the difference between spin locking and rotated displacement for blockade is evident. For spin 3/2, difference of photon blockade and spin lock becomes clearer. We show experimentally measured Wigner functions at two different times (Fig. S2(e)) to show the difference between spin locking and continued rotation. This is accompanied by an ideal simulation of the spin and photon blockade dynamics.

B. Detuned Spin Rotations (Spin Chevrons)

For two-level qubit system, the qubit drive frequency can be slightly detuned in a time Rabi experiment, to create a qubit chevron experiment where we can see the Rabi rate changing with detuning. For spins created in our cavity we can also detune the cavity drive and see the change in our oscillation rate. A spin 1/2 system is essentially a two-level qubit and a detuning on the cavity drive creates a chevron pattern as shown in Fig. S3(a,e). For spin 1, the oscillation rate and population in cavity also change with the detuning. Simulations of our system match experimental data as shown in Fig. S3(b-d,f-h). These chevron plots are a necessary step for calibrating the correct frequency for resonant cavity drive in presence of frequency comb on cavity and qubit. We found that in the presence of two-cavity drives the frequency at which the population of P_0 is maximally reduced and P_{2J} is maximally increased for spin J is about 9 kHz less than the cavity frequency calibrated using cavity state revival technique [1]. This detuning is observed to be the same for all spins in experiment, so we conclude that this originates from having two cavity drives and not a stark shift because of having multi-frequency qubit drive.

C. Qubit drive phase variation for spin 1

Here we vary the phase on the qubit drive at frequency $f_q + 2\chi$ and check the dynamics of cavity population of the Fock states $|0\rangle, |1\rangle, |2\rangle$. At phase $= \pi$, the matrix element for transition from $|1\rangle$ to $|2\rangle$ is set to zero, and hence the system is reduced to a spin 1/2 system where we only see oscillations between $|0\rangle$ and $|1\rangle$.

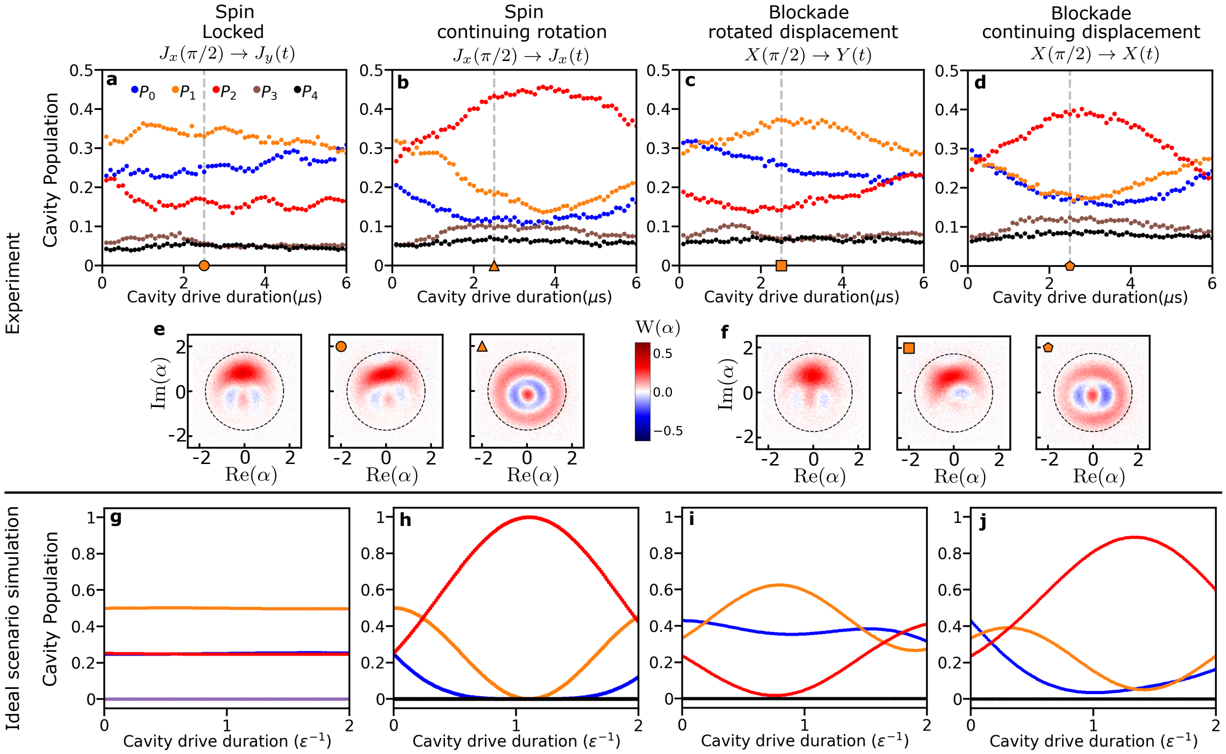

FIG. S1. **Spin Locking, spin 1:** We initialize a state on the equator of a spin 1 Bloch sphere by applying a $\hat{J}_x$ rotation and then (a) apply a $\hat{J}_y$ rotation and the cavity population is probed at different duration of the $\hat{J}_y$ drive. Since the created state is on the $\hat{J}_y$ axis, ideally the population should not change. (b) apply a $\hat{J}_x$ rotation and probe the population at different duration of the $\hat{J}_x$ drive. For a simple 3-level blockade, we can also prepare the state at one quarter of the time when population in Fock state 0 returns to maximum, and then (c) drive it along an axis that is rotated by 90 degrees or, (d) drive it along the same axis to probe the population at different times. (e) Experimentally measured Wigner functions for a spin state created on the equator and the states created after 2.4 µs of $\hat{J}_y$ and $\hat{J}_x$ drive respectively. (f) Experimentally measured Wigner functions for a created on the equator using 3-level blockade and the states created after 2.4 µs of drives on a 90 degree rotated axis and the original axis. (g) - (j) show the simulated probabilities of different cavity states for the cases of spin locking, continued rotation, rotated displacement, and continued displacement (corresponding to experiments in (a)- (d)) achieved by our protocol in an ideal scenario.

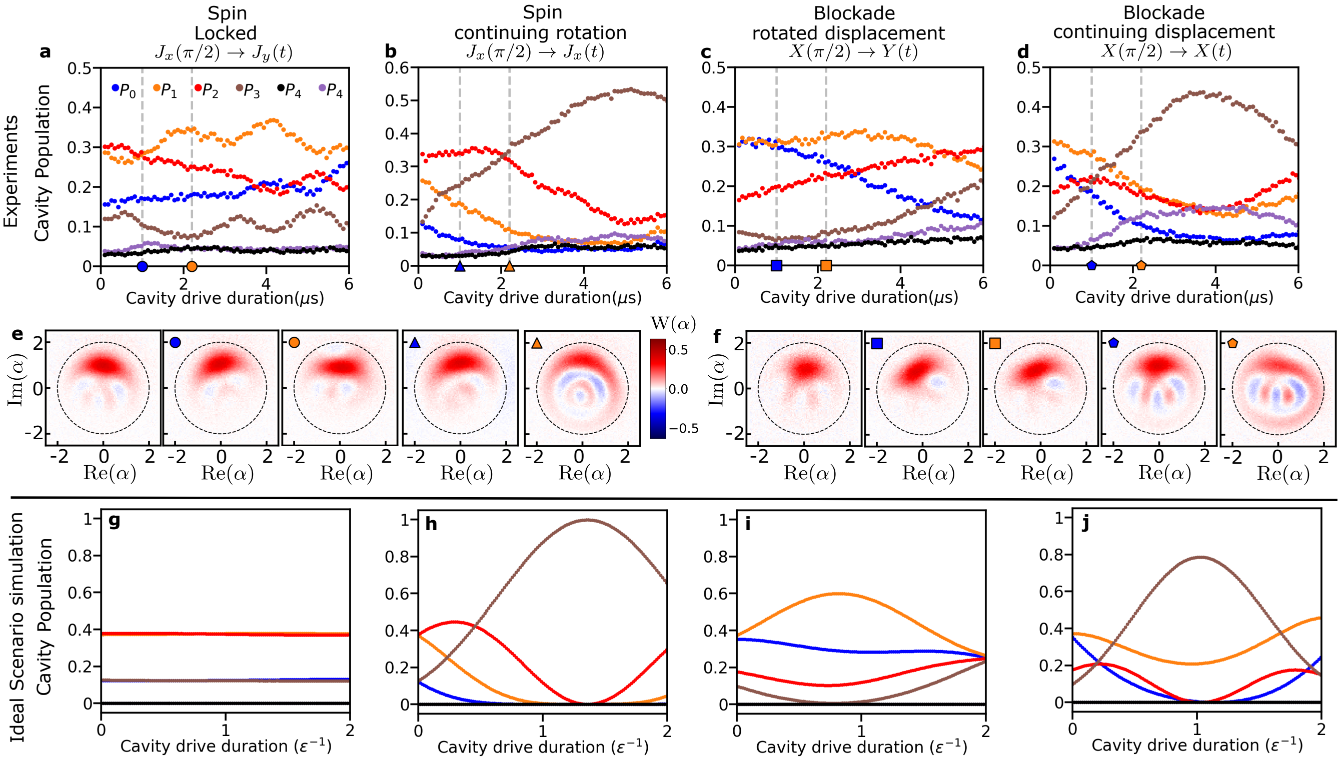

FIG. S2. **Spin Locking spin 3/2:** Create a state on the equator of a spin 3/2 Bloch sphere by applying a $\hat{J}_x$ rotation and then (a) apply a $\hat{J}_y$ rotation and the cavity population is probed at different duration of the $\hat{J}_y$ drive. Since the created state is on the $\hat{J}_y$ axis, ideally the population should not change. (b) apply a $\hat{J}_x$ rotation and probe the population at different duration of the $\hat{J}_x$ drive. For a simple 3-level blockade, we can also prepare the state at one quarter of the time when population in Fock state 0 returns to maximum, and then (c) drive it along an axis that is rotated by 90 degrees or, (d) drive it along the same axis to probe the population at different times. (e) Experimentally measured Wigner functions for a spin state created on the equator and the states created after 1 µs and 2.2 µs of $\hat{J}_y$ and $\hat{J}_x$ drive respectively. (f) Experimentally measured Wigner functions for a created on the equator using 3-level blockade and the states created after 1 µs and 2.2 µs of drives on a 90 degree rotated axis and the original axis. (g) - (j) show the simulated probabilities of different cavity states for the cases of spin locking, continued rotation, rotated displacement, and continued displacement (corresponding to experiments in (a)- (d)) achieved by our protocol in an ideal scenario..

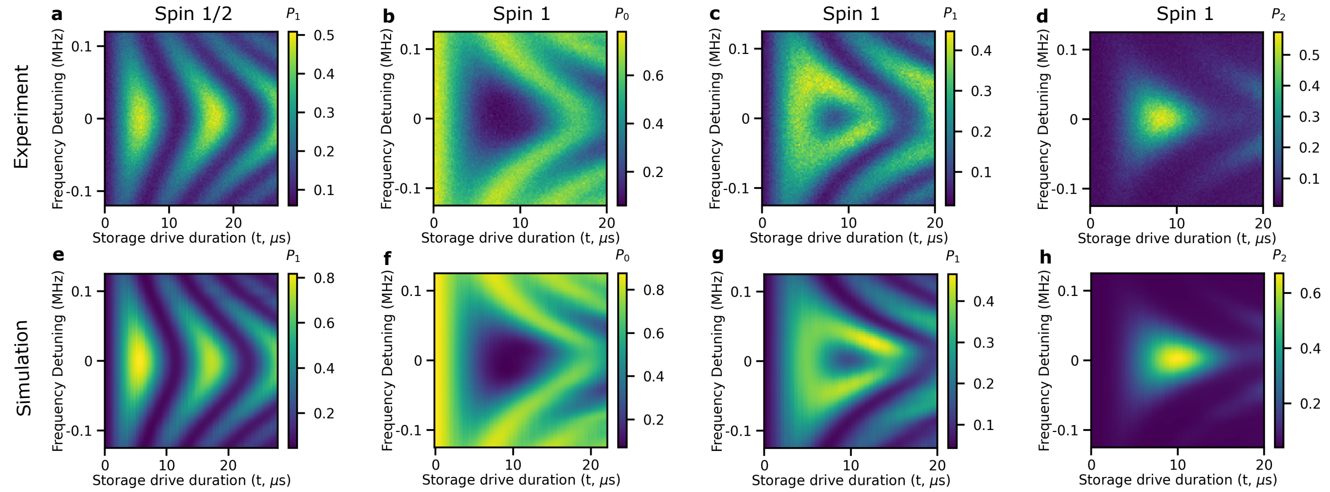

FIG. S3. **Spin Chevron:** Both cavity drives for spin coherent rotation are detuned to create a chevron-like plot for spins. Spin Chevron plots for (a) spin 1/2, probing the population of Fock state $|1\rangle$, (b) spin 1, probing the population of Fock state $|0\rangle$. (c) spin 1, probing the population of Fock state $|1\rangle$, (d) spin 1, probing the population of Fock state $|2\rangle$. e-h are corresponding simulations using experimental parameters.

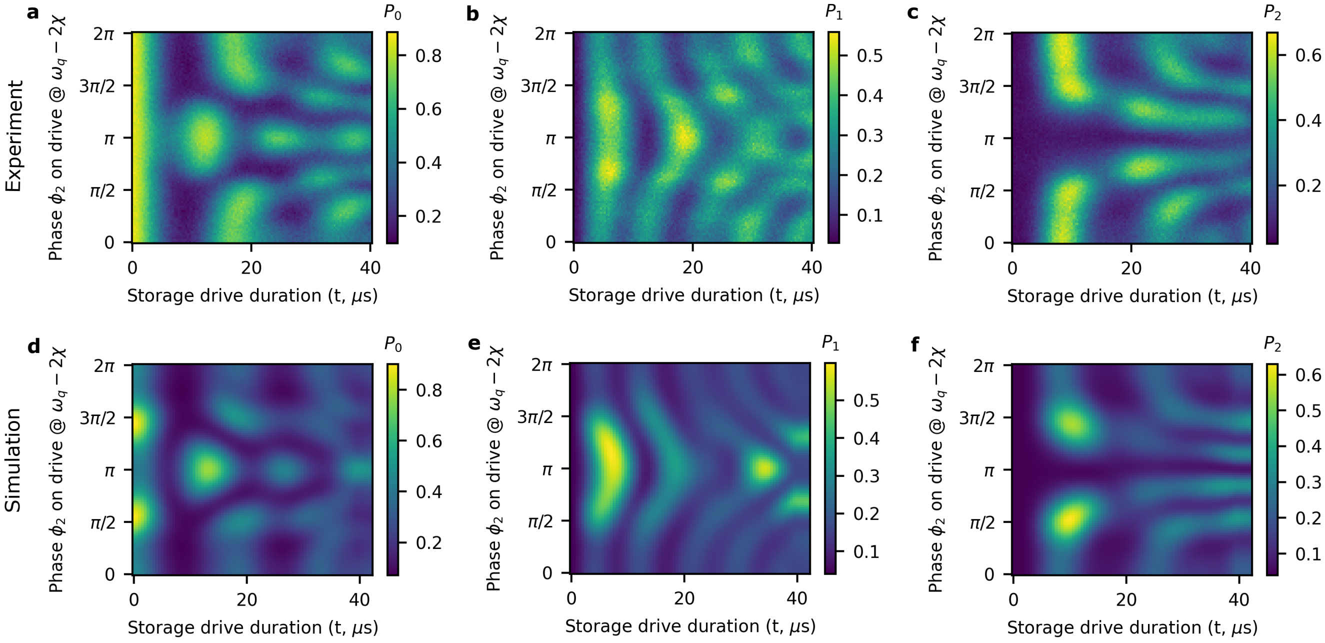

FIG. S4. **Spin 1 phase variation:** Phase ϕ_2 on the qubit drive at frequency $\omega_q + 2\chi$ is varied from 0 to 2π and the population in cavity is probed. As phase is changed, the oscillation period and shape changes. Particularly at phase π, there is no population in $N = 2$ cavity state. Hence, the spin 1 system is reduced to a spin 1/2 system.

II. SPIN WIGNER FUNCTION

A. Theoretical construction

We show in this section that the spin rotations demonstrated above can be used to measure the spin Wigner function. For a standard harmonic oscillator, the Wigner function associates to each state ρ a function in phase space (q, p) that can be computed from

$$\begin{aligned} W_\rho(q,p) &= \mathrm{Tr}\left[\hat{\Delta}(q,p)\rho\right], \\ \hat{\Delta}(q,p) &= 2\hat{D}(q,p)\mathrm{e}^{i\pi\hat{a}^\dagger\hat{a}}\hat{D}^\dagger(q,p), \end{aligned} \tag{1}$$

where we have defined $\hat{D}(q,p) = \exp(i\hat{x}p - i\hat{p}q)$. Measuring the Wigner function amounts to displacing the state by $(-q, -p)$ and then measuring the photon number parity. The definition above differs from the usual definition by a factor $1/2\pi$ in order to correspond to the $J \to \infty$ limit of the spin Wigner function below. The bounds of our spin Wigner function definition is shown in fig. II A.

For a spin state, a spin Wigner function can be defined analogously, where the linear displacements are replaced by spin rotations $\hat{R}_J(\theta,\phi) = \mathrm{e}^{i\theta(\cos\phi\hat{J}_x^{(J)} + \sin\phi\hat{J}_y^{(j)})}$ and the parity operator by

$$\begin{aligned} \hat{\Delta}(\theta,\phi) &= \hat{R}_J(\theta,\phi)\hat{\Delta}\hat{R}_J^\dagger(\theta,\phi), \\ \hat{\Delta} &= \sum_{m=-J}^{J}\sum_{l=0}^{2J}\frac{2l+1}{\sqrt{2J(2J+1)}}C_{Jm,l0}^{Jm}\left|m+J\right\rangle\left\langle m+J\right|, \\ &= \sum_{m=-J}^{J}\Delta_m\left|m+J\right\rangle\left\langle m+J\right|, \end{aligned} \tag{2}$$

where the $C_{j_1m_1j_2m_2}^{JM}$ are the Clebsch-Gordan coefficients. The spin Wigner function is correspondingly defined as [2–4]

$$W_\rho^{(J)}(\theta,\phi) = \mathrm{Tr}\left[\hat{\Delta}(\theta,\phi)\rho\right] \ . \tag{3}$$

The map $W : O \to W_O^{(J)}$ respects the Stratonovich-Weyl postulates

1. Linearity: W is linear and one-to-one
2. Reality:
$$W_{O^\dagger}^{(J)} = \left(W_O^{(J)}\right)^* \ . \tag{4}$$
3. Standardization: Defining $d\Omega = \sin\theta d\theta d\phi$, we have
$$\mathrm{Tr}(O) = \frac{2J+1}{4\pi}\int_{J^2} d\Omega\, W_O^{(J)}(\theta,\phi) \ . \tag{5}$$
4. Traciality: for two operators O and P
$$\mathrm{Tr}(OM) = \frac{2J+1}{4\pi}\int_{J^2} d\Omega\, W_O^{(J)}(\theta,\phi)W_M^{(J)}(\theta,\phi) \ . \tag{6}$$
5. Covariance:
$$W_{\hat{R}_S(\alpha,\beta)O\hat{R}_S^\dagger(\alpha,\beta)}^{(J)}(\theta,\phi) = W_O^{(J)}(\theta',\phi'), \tag{7}$$
where $\vec{n}' = (\sin\theta'\cos\phi', \sin\theta'\sin\phi', \cos\theta') = \left[R(\hat{R}_J(\alpha,\beta))\right]^{-1} \cdot (\sin\theta\cos\phi, \sin\theta\sin\phi, \cos\theta)$ with $R(U)$ the $SO(3)$ representation of the $SU(2)$ element $\hat{R}_J(\alpha,\beta)$.

We can measure this spin Wigner using SU(2) spin rotations and Fock-dependent qubit rotations. Let us redefine the Wigner function as

$$\begin{aligned} W_\rho(\theta,\phi) &= \mathrm{Tr}\left[\hat{\Delta}\rho_{\theta,\phi}\right] \\ \rho_{\theta,\phi} &= \hat{R}_J^\dagger(\theta,\phi)\rho\hat{R}_J(\theta,\phi) \ . \end{aligned} \tag{8}$$

We can rewrite the matrix elements of $\hat{\Delta}$ with

$$\begin{aligned} \gamma_m &= \frac{\Delta_m - \Delta_{\mathrm{min}}}{\Delta_{\mathrm{max}} - \Delta_{\mathrm{min}}} \\ \hat{\gamma} &= \sum_m \gamma_m\left|m\right\rangle\left\langle m\right|, \\ \hat{\Delta} &= \Delta_{\mathrm{min}} + (\Delta_{\mathrm{max}} - \Delta_{\mathrm{min}})\hat{\gamma}, \end{aligned} \tag{9}$$

where we have defined $\Delta_{\mathrm{min}} = \min(\{\Delta_m\})$ and $\Delta_{\mathrm{max}} = \max(\{\Delta_m\})$ Here, importantly, the eigenvalues of $\hat{\gamma}$ are given by $\gamma_m \in [0,1]$. We can thus define a set of angles θ_m such that

$$\cos^2\left(\frac{\theta_m}{2}\right) = \gamma_m \ . \tag{10}$$

We can measure the Wigner function through a qubit measurement after the pulse

$$\hat{U}_\gamma = \sum_m \hat{R}_x(\theta_m)\otimes\left|m\right\rangle\left\langle m\right| \ , \tag{11}$$

which rotates the qubit by a different angle for each Fock state $|m\rangle$, where the angle depends on γ_m. The probability of measuring $|g\rangle$ after the (inverse) SU(2) rotation and the pulse $\hat{U}_\gamma$, assuming that the qubit is initialized in $|g\rangle$, is

$$\begin{aligned} \langle\left|g\right\rangle\left\langle g\right|\otimes\mathbb{I}\rangle &= \mathrm{Tr}\left[\hat{U}_\gamma(\left|g\right\rangle\left\langle g\right|\otimes\rho_{\theta,\phi})\hat{U}_\gamma^\dagger(\left|g\right\rangle\left\langle g\right|\otimes\mathbb{I})\right] \\ &= \sum_m \left|\left\langle e\right|\hat{U}_\gamma\left|g\right\rangle\right|^2\mathrm{Tr}[\rho_{\theta,\phi}\left|m\right\rangle\left\langle m\right|] \\ &= \sum_m \cos^2\left(\frac{\theta_m}{2}\right)\mathrm{Tr}[\rho_{\theta,\phi}\left|m\right\rangle\left\langle m\right|] \\ &= \langle\hat{\gamma}\rangle \ . \end{aligned} \tag{12}$$

Rescaling this probability by $(\gamma_{\mathrm{max}} - \gamma_{\mathrm{min}})$ and adding γ_{min} gives us $W_\rho(\theta,\phi)$.

In order to symmetrize the effect of readout errors, the expectation value of $\hat{\Delta}$ can also be decomposed as

$$\begin{aligned} \eta_m &= \frac{\Delta_{\mathrm{max}} - \Delta_m}{\Delta_{\mathrm{max}} - \Delta_{\mathrm{min}}} \\ \hat{\eta} &= \sum_m \eta_m\left|m\right\rangle\left\langle m\right|, \\ \hat{\Delta} &= \Delta_{\mathrm{max}} - (\Delta_{\mathrm{max}} - \Delta_{\mathrm{min}})\hat{\eta}. \end{aligned} \tag{13}$$

Accordingly, we can measure this operator by defining

$$\cos^2\left(\frac{\beta_m}{2}\right) = \eta_m \ , \tag{14}$$

and we can measure the Wigner function by measuring the qubit population in the $|g\rangle$ state after the pulse

$$\hat{U}_\eta = \sum_m \hat{R}_x(\beta_m) \otimes |m\rangle\langle m| \ . \tag{15}$$

B. Experimental implementation

In this section we demonstrate that the spin Wigner functions can be experimentally measured as described in App. II A. The schematic pulse sequence is shown in Fig. S6. First, we choose a qubit drive duration for the experiment based on Appendix C2 and Fig. A3. The first cavity drive is used to prepare the state we want to probe. For Fock state $|0\rangle$ and $|1\rangle$ we do not need this first drive as cavity $|0\rangle$ is prepared by having an idle period much longer than the cavity lifetime (T_1) and $|1\rangle$ is prepared using a conventional photon blockade procedure. The second cavity drive is used to accomplish a spin rotation for angle θ around an axis with angle ϕ with respect to the X axis. As we do for the spin cat gates, a ϕ rotation is accomplished by a frame rotation of the cavity drive and a θ rotation is achieved by varying the duration of the cavity drive. After the qubit drive ends we disentangle the qubit from cavity using SNAP gate that consists two consecutive number-selective π pulses on the qubit for a total duration of 2 µs. Then we readout the qubit state and store it for post-processing. Finally, we do number-selective qubit rotations and readout the final state of the qubit. The probability of finding the qubit in ground state (P_g) directly relates to the spin Wigner function.

For comparison to bosonic Wigner measurements, the spin rotation is analogous to displacement operation and the number-selective qubit rotations are analogous to the parity measurement. For symmetrizing errors during spin rotations, we do two different number-selective qubit rotations. For the first case, we do the θ_m rotations on the qubit following Eq. 10 and define the spin Wigner function as

$$W^{(1)}_{\text{spin}}(\theta,\phi) = \Delta_{\min} + P_g(\Delta_{\max} - \Delta_{\min}) \tag{16}$$

In a second experiment, we do β_m rotations on the qubit following Eq. 14 and define the spin Wigner as

$$W^{(2)}_{\text{spin}}(\theta,\phi) = \Delta_{\max} - P_g(\Delta_{\max} - \Delta_{\min}) \tag{17}$$

Finally, in a post-processing we select the cases where our first readout measured the qubit in ground state (implying the spin rotation was successful) and then average the two spin Wigner functions measured above to get the error-symmetrized spin Wigner function.

$$W_{\text{spin}}(\theta,\phi) = (W^{(1)}_{\text{spin}}(\theta,\phi) + W^{(2)}_{\text{spin}}(\theta,\phi))/2 \tag{18}$$

Spin Wigner functions measured this way are shown in Fig. S6 for spin 1: Fock state $|0\rangle$, $|1\rangle$, and a spin coherent state on the equator of spin 1 Bloch sphere. Since our spin rotations suffer from errors, the measured spin Wigner functions are noisy and imperfect, with poor contrast.

---

[1] K. S. Chou, *Teleported operations between logical qubits in circuit quantum electrodynamics*, Ph.D. thesis, Yale University (2018).

[2] R. L. Stratonovich, On distributions in representation space, Journal of Experimental and Theoretical Physics **4**, 891 (1957).

[3] G. S. Agarwal, Relation between atomic coherent-state representation, state multipoles, and generalized phase-space distributions, Physical Review A **24**, 2889 (1981).

[4] B. Koczor, R. Zeier, and S. J. Glaser, Continuous phase-space representations for finite-dimensional quantum states and their tomography, Physical Review A **101**, 022318 (2020).

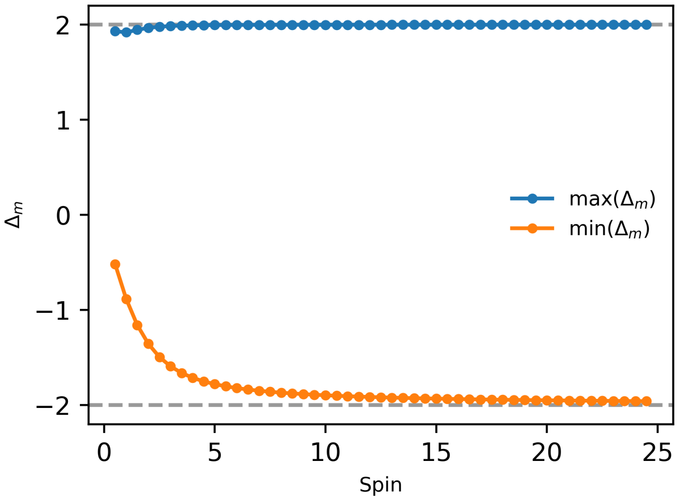

FIG. S5. **Limits of spin Wigner function:** The theoretically possible maximum and minimum values of spin Wigner function as a function of the size of the spin. As the spin size becomes large (or tends to infinite), the maximum and minimum values tend to ±2.

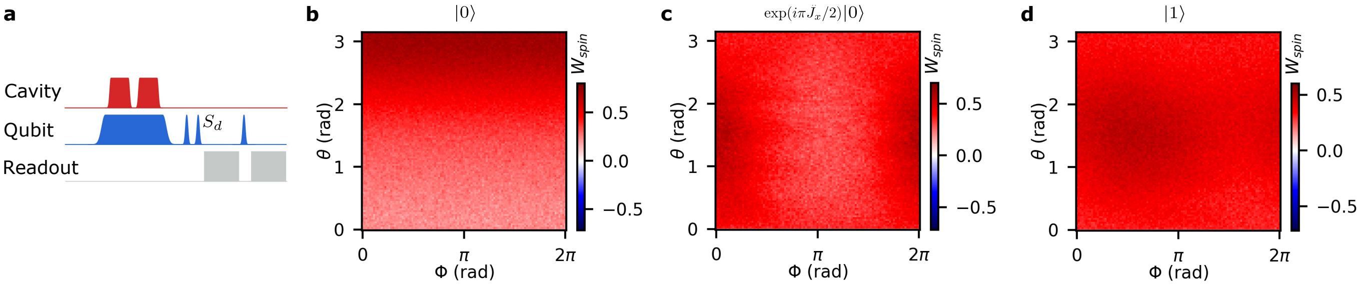

FIG. S6. **Spin Wigner:** (a) Pulse schematic for measuring the spin Wigner function for Spin 1. (b-d) Spin Wigner functions for (b) Fock state $|0\rangle$, (c) spin coherent state on the equator, (d) Fock state $|1\rangle$, which is also a equatorial spin cat state. Due to infidelities of spin rotations and measurements, the contrast of spin Wigner function is poor. So we had to scale the colorbar differently for better visibility in (b-d).